Entangling power of symmetric two-qubit quantum gates and three-level operations

D. Morachis Galindo⬤ and Jesús A. Maytorena⬤

Departamento de Física, Centro de Nanociencias y Nanotecnología,
Universidad Nacional Autónoma de México, Apartado Postal 14, 22800 Ensenada, Baja California, México

The capacity of a quantum gate to produce entangled states on a bipartite system is quantified in terms of the entangling power. This quantity is defined as the average of the linear entropy of entanglement of the states produced after applying a quantum gate over the whole set of separable states. Here we focus on symmetric two-qubit quantum gates, acting on the symmetric two-qubit space, and calculate the entangling power in terms of the appropriate local invariant. A geometric description of the local equivalence classes of gates is given in terms of the su(3) Lie algebra root vectors. These vectors define a primitive cell with hexagonal symmetry on a plane, and through the Weyl group the minimum area on the plane containing the whole set of locally equivalent quantum gates is identified. We give conditions to determine when a given quantum gate produces maximally entangled states from separable ones (perfect entanglers). We find that these gates correspond to one-fourth of the whole set of locally distinct quantum gates. The formalism developed here is applicable to general three-level systems. Via the Majorana representation, qutrit transformations can be regarded as having entangling power and hence classified as perfect and nonperfect entanglers and be grouped into local-equivalence classes of the associated symmetric two-qubit space. The results are illustrated by an anisotropic Heisenberg model, the Lipkin-Meshkov-Glick model, and two coupled quantized oscillators with cross-Kerr interaction, which we use to obtain three-level gates relevant in qutrit quantum computation.

I. INTRODUCTION

Entanglement is a purely quantum-mechanical phenomenon that is essential to achieving universal quantum computation based on interacting qubits systems [1]. Quantum logic gates are the building blocks to perform quantum algorithms, where the generation of entangled states from a separable set of states is mandatory to achieve the desired results [2].

Most of the proposed quantum computer architectures are based on multiqubit processors. Nevertheless, there are also proposals that use higher-dimensional systems called qudits, which have the advantage of reducing the number of physical entities required to perform calculations [3]. Among these are three-level systems, called qutrits, which are the smallest systems that may exhibit purely quantum correlations such as contextuality [4], and they have been used to construct three-level quantum gates [5,6]. Qutrits may be emulated by a two-qubit system symmetric under particle exchange. This allows us to think of many three-level transformations in terms of operations on the symmetric two-qubit symmetric space.

Within the Majorana representation [7,8], symmetric two-qubit states appear as two points ("stars") on the unit sphere. It can be shown that the distance between the two stars maps bijectively to the concurrence [9]. States with maximally separated stars correspond to Bell states, while states with stars at the same position are separable. This allows one to think of any transformation between these kinds of states as rigid or nonrigid motion of the associated Majorana constellation, where the latter (former) does (does not) change the entangle-

ment of states. Whenever there is no possibility for confusion, we will refer to a two-qubit symmetric state (space) as a symmetric state (space) only.

Since many transformations on symmetric (three-level) spaces involve changing the entanglement (distance between the Majorana stars), it is important to quantify the capacity of quantum gates to generate it. Such a quantity is called the entangling power [10]. It is defined as the average linear entropy of the states produced by a quantum gate $\hat{V}$ acting on the manifold of all separable states. For general two-qubit quantum gates (TQQGs) the entangling power can be compactly written in terms of a two-qubit gate local invariant [11] and sets values to classify TQQGs as perfect entanglers [11,12], that is to say, a quantum gate that at least produces a Bell state out of the set of separable states. Nevertheless, these expressions do not quantify the entangling power of gates acting irreducibly on the symmetric subspace, called symmetric quantum gates (SQGs), because they involve a contribution from separable nonsymmetric states. Here we will derive the appropriate expression of the entangling power for SQGs and find an onset value above which they can be classified as perfect entanglers.

As noted by Zhang *et al.* [13], distinct TQQGs can be put together into sets whose elements differ by local transformations, called local equivalence classes (LECs). By group-theoretic methods, the authors were able to represent all LECs of TQQG classes on a tetrahedron and showed that half of its volume is occupied by perfect entanglers. Motivated by Ref. [13], we develop a geometric description of the LECs of symmetric gates. We find that these are characterized by a

periodic set of points on a plane, displaying hexagonal symmetry with lattice vectors determined by the su(3) algebra root vectors. This allows us to identify a minimum extension where all inequivalent LECs of SQGs are located, known as the Weyl chamber, and to show that one-fourth of it is occupied by perfect entanglers.

This geometric approach and the entangling power concept are relevant to study operations in general three-level systems. This is a major motivation for the present work. For example, a natural question that arises in a qutrit-based quantum computation protocol is whether a set of quantum gates can transform the basis kets into each other [5]. As will be explained in the next section, this is only possible as long as the qutrit operations at hand have the ability to generate Bell-type states from separable states in the associated symmetric space. Three-level quantum gates with such a property need to forcefully have a minimum entangling power that will be determined later and can be located at a special zone in the Weyl chamber. The theoretical development presented here provides further understanding of general three-level transformations. These are of fundamental importance, for example, in the study of coherent population transfer [14–16] and the dynamics of spin-1 Bose-Einstein condensates [17–19] and might be useful for implementing quantum computation or information tasks based on qutrit processors, which are an active research field [20–25].

This paper is organized as follows. In Secs. II and III we present brief descriptions of the Majorana representation and of the Cartan decomposition of TQQGs and how it is related to SQGs, respectively. In Sec. IV the appropriate local invariant for SQGs is defined. Section V is devoted to analyzing the entangling power and using it to classify SQGs as perfect entanglers. In Sec. VI the developed formalism is applied to some example models involving two interacting spins [26], the three-level Lipkin-Meshkov-Glick (LMG) model from nuclear physics [27], and two coupled quantized oscillators through the cross-Kerr effect of quantum optics [28]. Section VII is devoted to conclusions. Appendix A includes the derivation of the entangling power formula and Appendix B contains a theorem which allows us to classify SQGs as perfect entanglers.

II. MAJORANA STELLAR REPRESENTATION

The Majorana representation is a geometric depiction of quantum states contained in a finite Hilbert space, which can give insight into their entangling properties [9]. The idea behind its construction is to obtain a complex polynomial out of the probability amplitudes that define a state for some fixed basis. The roots of such a polynomial can be represented by points in the Argand diagram and mapped into a sphere by stereographic projection [7,9]. For a quantum state $|\psi\rangle = \sum a_k |k\rangle$ in an n-dimensional Hilbert space, the Majorana polynomial is given by

$$\sum_{k=1}^{n} \frac{(-1)^k a_k}{\sqrt{(n-k)!k!}} z^{n-k} = 0. \tag{1}$$

The solutions $\{z_k\}$ lie on the complex plane and their projection onto the Riemann sphere is made by the association $z_k =$
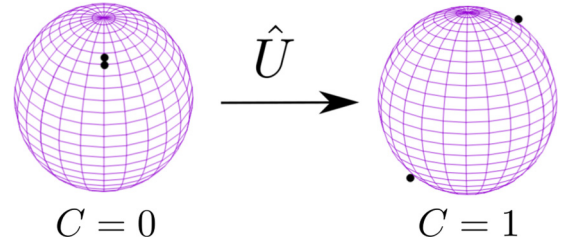

FIG. 1. Action of a quantum gate on a separable initial state (with concurrence $C = 0$) which ends up as a Bell state ($C = 1$) on the Majorana sphere. A quantum gate with this property is referred to as a perfect entangler

$\tan(\theta_k/2)e^{i\phi_k}$. Each root z_k is called a Majorana star, while the whole set of roots is referred to as the Majorana constellation of the quantum state $|\psi\rangle$. In fact, any two quantum states with the same constellation are equivalent, up to a global phase, which makes this representation a good description of their projective space.

The $(n + 1)$-dimensional Hilbert space has a bijection onto the space of n qubits with particle permutation symmetry. This implies that symmetric qubit states have associated Majorana constellations. The z_k roots define the components of a ket state in the symmetric space, by the relation

$$|\psi\rangle = \frac{1}{\sqrt{n!N_n}} \sum_{P} |u_{P(1)}, u_{P(2)}, \ldots, u_{P(n)}\rangle, \tag{2}$$

where $|u_i\rangle$ represents the one-qubit state $(\cos \frac{\theta_i}{2}, e^{i\phi_i} \sin \frac{\theta_i}{2})^T$; the symbol P denotes all the possible permutations of the $|u_i\rangle$ states and N_n is a normalization coefficient [29]. Thus, the Majorana constellation serves as the mapping between an $(n + 1)$-dimensional Hilbert space and the space of n-qubit symmetric wave functions.

For symmetric two-qubit states, the Majorana constellation consists of two stars. As shown in Ref. [9], their concurrence is proportional to the square of the chordal distance between the stars. This implies that states with zero concurrence have their Majorana stars at the same position, that is, they have degenerate stars. In contrast, maximally entangled states have stars occupying antipodal positions on the sphere. For monopartite three-level systems we may also speak of entangled states as those whose Majorana stars are not co-incident.

Along the same line of thought, three-level transformations will be referred to as entangling as long as they can produce a state with nondegenerate Majorana stars from a state with a degenerate constellation. Figure 1 illustrates a separable state (degenerate constellation) which, after being acted on by a SQG, ends up as a fully entangled state (antipodal Majorana stars); such unitary transformations are called perfect entanglers and will be discussed later in the paper. Consider a three-level system Hilbert space spanned by $|\pm1\rangle$ and $|0\rangle$ in the spin-1 angular momentum basis, where we have suppressed the index denoting the total angular momentum $j = 1$. The mapping to the symmetric space is given by the associations $|1\rangle, |-1\rangle, |0\rangle \rightarrow |0, 0\rangle, |1, 1\rangle, (|0, 1\rangle + |1, 0\rangle)/\sqrt{2}$, respectively, as suggested by the sum of angular momenta of two spin-$\frac{1}{2}$ particles. The symmetric states above follow from

Eq. (2) by taking $n = 2$. The first two states on the three levels correspond to separable states on the symmetric space and have degenerate Majorana constellations, while the third one corresponds to a Bell state and has stars on antipodal positions. Thus, a SQG (qutrit or three-level operation) converting $|\pm 1\rangle$ to $|0\rangle$ has to be a perfect entangler. Examples of these gates in three-level systems are some phase gates and the SWAP$_{12}$ and SWAP$_{23}$ gates, which have found applications in qutrit-based quantum computing [5]. The association between the angular momentum basis and the symmetric two-qubit states above will be extensively used in the rest of the paper, because it will allow us to translate entanglement and related concepts to three-level systems.

III. CARTAN DECOMPOSITION OF UNITARY TWO-QUBIT AND THREE-LEVEL TRANSFORMATIONS

The whole set of transformations on the Hilbert space of two qubits can be classified as local and nonlocal. Local operations are those physical processes that act separately only on one component of the bipartite system and, as a consequence, do not change the entanglement properties of the state. Local two-qubit gates can always be written as a tensor product of one-qubit operations

$$\hat{V}^{(12)} = \hat{V}^{(1)} \otimes \hat{V}^{(2)}, \qquad (3)$$

which belong to the SU(2) ⊗ SU(2) Lie group. We will restrict $\hat{V}$ to denote transformations on the two-qubit space, not necessarily symmetric.

In general, TQQGs that are elements of the set SU(4) that cannot be written as in (3) are called nonlocal. There is a very concise way of writing every element of SU(4) given by the *KAK* decomposition of the group. Namely, for every $\hat{V} \in$ SU(4), we have the identity [30]

$$\hat{V} = \hat{K}_1 \hat{A} \hat{K}_2, \qquad (4)$$

$$\hat{A} = \exp\left[\frac{i}{2} \sum_k c_k \hat{\sigma}_{x_k}^{(1)} \otimes \hat{\sigma}_{x_k}^{(2)}\right]. \qquad (5)$$

The $\hat{K}$ factors belong to the SU(2) ⊗ SU(2) Lie group; hence they are local. As usual, the $\hat{\sigma}_{x_k}$ operators denote the Pauli matrices, with $k = 1, 2, 3$ and $x_k = x, y, z$. The $\hat{A}$ factor contains the nonlocal part of the quantum gates and is given by the exponential of linear combinations of the operators $\hat{\sigma}_{x_i}^{(1)} \otimes \hat{\sigma}_{x_i}^{(2)}$. Two-qubit quantum gates that differ only by a $\hat{K}$ factor are said to be in the same local equivalence class. These set of operators span the Cartan subalgebra of the SU(4) Lie group, which is a maximally commuting subalgebra of su(4) [13]. It can be seen that the (c_1, c_2, c_3) coordinates have a period of π each, and thus the topological structure of the local equivalence classes is a 3-torus [13]. The $\boldsymbol{c} = (c_1, c_2, c_3)$ point will be called a geometrical point hereafter. For a more detailed discussion of the Cartan decomposition of SU(4) and its algebra, namely, the su(4) Lie algebra, see Ref. [13].

There is a special case of TQQGs that act irreducibly on the symmetric and antisymmetric two-qubit ket spaces. Therefore, if $\hat{V}^{(r)}$ is an element of such a special set, in which (r)

denotes a reducible representation, it has a matrix form

$$\hat{V}^{(r)} = \begin{pmatrix} \hat{U} & 0 \\ 0 & 1 \end{pmatrix}, \qquad (6)$$

where $\hat{U} \in$ SU(3) acts on any symmetric linear combination of the computational basis; $\hat{U}$ is thus the SQG we are interested in, as was said in the Introduction. The last factor acts on the antisymmetric Bell state $|\phi^-\rangle = \frac{1}{\sqrt{2}}(|01\rangle - |10\rangle)$.

Since reducible gates are a subgroup of SU(4), the Cartan decomposition holds for all elements of the form (6). Also, for reducible TQQGs, the Cartan decomposition is composed of reducible factors. To see this, first let us note that $\hat{A}$ is reducible, as will be seen in the next section. With this, it is readily shown that a sufficient condition for $\hat{V}$ to be reducible is that $\hat{K}$ be reducible. To show that reducibility of $\hat{V}$ implies the reducibility of $\hat{K}$, we use the Cartan decomposition of the SU(3) Lie group explained in Appendix A. This states that $\hat{U} \in$ SU(3) can be written as $\hat{k}_1 \hat{B} \hat{k}_2$, where $\hat{k}_i = e^{-i\theta_i \hat{\mathbf{n}}_i \cdot \hat{\boldsymbol{J}}}$ and $\hat{B}$ is the symmetric part of the $\hat{A}$ matrix expressed in the angular momentum basis. Hence we have

$$\begin{pmatrix} \hat{U} & 0 \\ 0 & 1 \end{pmatrix} = \begin{pmatrix} \hat{k}_1 & 0 \\ 0 & 1 \end{pmatrix} \begin{pmatrix} \hat{B} & 0 \\ 0 & 1 \end{pmatrix} \begin{pmatrix} \hat{k}_2 & 0 \\ 0 & 1 \end{pmatrix}.$$

The upper and lower off-diagonal elements are three-dimensional column and row vectors, respectively. When expressing each factor on the right-hand side of the equation above in the computational basis, one sees that the reducible matrices containing $\hat{k}$ map to $e^{-i(\theta/2)\hat{\mathbf{n}}\cdot\hat{\boldsymbol{\sigma}}} \otimes e^{-i(\theta/2)\hat{\mathbf{n}}\cdot\hat{\boldsymbol{\sigma}}}$, as shown in more detail in Appendix A.

IV. LOCAL INVARIANTS AND EQUIVALENCE CLASSES OF SYMMETRIC QUANTUM GATES

Two-qubit quantum gates that are equivalent up to a local gate factor [see Eq. (4)] have the same local invariants [13,31]. Local invariants for two-qubit quantum gates are determined by the set of eigenvalues of

$$\hat{M} = \hat{V}_B^T \hat{V}_B, \qquad (7)$$

where the label B indicates that the gate $\hat{V}$ is expressed in the Bell basis $B = \{|\psi^+\rangle, |\psi^-\rangle, |\phi^+\rangle, |\phi^-\rangle\}$. The transformation matrix between the Bell states and the computational basis, ordered as $\{|00\rangle, |01\rangle, |10\rangle, |11\rangle\}$, is

$$\hat{Q}^\dagger = \frac{1}{\sqrt{2}} \begin{pmatrix} 1 & 0 & 0 & 1 \\ 0 & i & i & 0 \\ i & 0 & 0 & -i \\ 0 & 1 & -1 & 0 \end{pmatrix}. \qquad (8)$$

Thus, the $\hat{V}$ in the Bell basis is given by $\hat{V}_B = \hat{Q}^\dagger \hat{V} \hat{Q}$. The Lie algebra of the local components of two-qubit quantum gate is isomorphic to the Lie algebra of the SO(4) group [13], through the map defined by Eq. (8). Thus, any two-qubit quantum gate in the Bell basis, whose decomposition is given by (4), becomes

$$\hat{V}_B = \hat{O}_1 \hat{F} \hat{O}_2, \qquad (9)$$

where $\hat{O}_{1,2} = \hat{Q}^\dagger \hat{K}_{1,2} \hat{Q} \in$ SO(4) and $\hat{F} = \hat{Q}^\dagger \hat{A} \hat{Q}$, which is diagonal in this basis. The Bell states $|\psi^+\rangle, |\psi^-\rangle, |\phi^+\rangle$, and
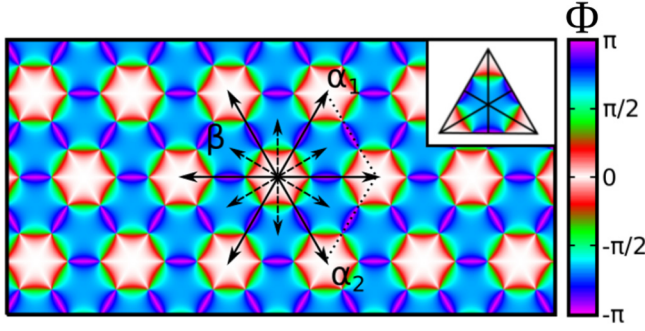
FIG. 2. Complex argument Φ of $\mathrm{Tr}\hat{m}$ in the O plane (13). The $\boldsymbol{\alpha}_1$ and $\boldsymbol{\alpha}_2$ are the root vectors of the su(3) Lie algebra. Every pair of antiparallel short arrows lies in a plane belonging to the set that generates the Weyl group. The inset shows a subcell divided into six slices, each one corresponding to a Weyl chamber.

$|\phi^-\rangle$ are thus eigenstates of the $\hat{A}$ matrix, with respective eigenvalues

$$\lambda_1 = e^{i(c_1-c_2+c_3)/2}, \tag{10a}$$

$$\lambda_2 = e^{i(c_1+c_2-c_3)/2}, \tag{10b}$$

$$\lambda_3 = e^{i(-c_1+c_2+c_3)/2}, \tag{10c}$$

$$\lambda_4 = e^{-i(c_1+c_2+c_3)/2}. \tag{10d}$$

The eigenvalues of the matrix $\hat{M}$ are determined by the quantities $(\mathrm{Tr}\,\hat{M})^2$ and $(\mathrm{Tr}\,\hat{M})^2 - \mathrm{Tr}\,\hat{M}^2$, which in turn serve to define the local invariants of two qubit quantum gates, namely,

$$G_1 = \tfrac{1}{16}(\mathrm{Tr}\hat{M})^2, \tag{11a}$$

$$G_2 = \tfrac{1}{4}[(\mathrm{Tr}\hat{M})^2 - \mathrm{Tr}\hat{M}^2]. \tag{11b}$$

Thus, distinct TQQGs having the same local invariants are said to be locally equivalent.

Reducible TQQGs can be expressed as in Eq. (6) and their action on the symmetric subspace only depends on $\hat{U}$. The local invariant of the symmetric part of the gate is determined by the eigenvalues of

$$\hat{m} = \hat{U}_B^T \hat{U}_B \tag{12}$$

and is then independent of the λ_4 eigenvalue. Since we have considered special unitary gates, this implies that

$$c_1 + c_2 + c_3 = 0. \tag{13}$$

Had we regarded general unitary gates, removing the extra phase factor would lead to the same condition above; thus all LECs can be located in the plane defined in (13).

The secular equation of the matrix $\hat{m}$ is given by

$$\lambda^3 - \mathrm{Tr}(\hat{m})\lambda^2 - \mathrm{Tr}^*(\hat{m})\lambda - 1 = 0, \tag{14}$$

where we have used (9) and (10) to simplify the related factor $\mathrm{Tr}^2(\hat{m}) - \mathrm{Tr}(\hat{m}^2)$. Thus, for SQGs the eigenvalues of $\hat{m}$ are determined by its trace. In this case, there is only one local invariant which determines the LECs, in clear contrast to general TQQGs, where LECs are determined by two invariants G_1 and G_2. The argument of $\mathrm{Tr}\hat{m}$ is plotted in Fig. 2.

We define the SQGs local invariant as

$$G = \tfrac{1}{9}[\mathrm{Tr}(\hat{m})]^2. \tag{15}$$

The norm of G can be compactly written in terms of the (c_1, c_2, c_3) vector as

$$|G| = 1 - \tfrac{4}{9}[\sin^2(c_{12}) + \sin^2(c_{13}) + \sin^2(c_{32})], \tag{16}$$

where c_{ij} is shorthand for $c_i - c_j$. Thus, distinct SQGs having the same value of G are said to be locally equivalent.

The whole extension of the O plane (13) has more information than is actually needed, given the periodicity the matrix $\hat{A}$ [Eq. (5)] up to local gate factors $\hat{K}$. Consider the vectors $\boldsymbol{\alpha}_1 = (-\pi, 0, \pi)$ and $\boldsymbol{\alpha}_2 = (0, \pi, -\pi)$ lying on the O plane. The $\hat{A}$ matrix is obviously periodic along these directions. Also, the angle between them is $2\pi/3$. Thus, SQGs whose geometrical points differ by a $n\boldsymbol{\alpha}_1 + m\boldsymbol{\alpha}_2$ translation ($n, m \in \mathbb{Z}$) are locally equivalent, and the whole set of local equivalent classes can be found within the hexagonal primitive cell spanned by $\boldsymbol{\alpha}_1$ and $\boldsymbol{\alpha}_2$, which is displayed in Fig. 2 by the area between these vectors and the dotted lines. The vectors $\boldsymbol{\alpha}_1$ and $\boldsymbol{\alpha}_2$ are the root vectors of the su(3) Lie algebra and the set $\{\pm\boldsymbol{\alpha}_1, \pm\boldsymbol{\alpha}_2, \pm(\boldsymbol{\alpha}_1 + \boldsymbol{\alpha}_2)\}$ (solid arrows in Fig. 2) form the root space of the algebra [32].

Consider the reflection matrix $(\hat{\sigma}_{\hat{\boldsymbol{\beta}}})_{ij} = \delta_{ij} - 2\beta_i\beta_j/\beta^2$ ($i, j = x, y, z$) on the plane normal to the unit vector $\hat{\boldsymbol{\beta}}$, which is obtained from any vector lying between two successive root vectors (dotted arrows). It can be checked that the effect of $\hat{\sigma}_{\hat{\boldsymbol{\beta}}}$ is to permute and complex conjugate the eigenvalues of the $\hat{m}$ matrix. From Fig. 2 it can be seen that reflection on the plane normal to the vertical $\hat{\boldsymbol{\beta}}$ vectors interchanges the triangles composing the unit cell depicted there. This means that knowledge of $\mathrm{Tr}\hat{m}$ on a subcell determines its value on the other subcell by complex conjugation, and thus all LECs can be located in just one subcell.

Reflection on the planes normal to the root vectors generates the Weyl group of su(3); the corresponding reflection matrices are given by $\hat{\sigma}_{\hat{\boldsymbol{\alpha}}}$, where $\hat{\boldsymbol{\alpha}}$ is a normalized root vector. The action of this group on the $\hat{A}$ matrix is permuting its eigenvalues and thus leaves the character of $\hat{m}$ invariant. As in the general two-qubit case [13], the Weyl group allows us to define a minimum extension containing the whole set of local equivalence classes, called the Weyl chamber [13,32]. By bisecting one triangle of the primitive cell by the planes normal to the root space we get the inset of Fig. 2. Every slice of the triangle contains all the local-equivalence classes of SQGs up to complex conjugation and represents a Weyl chamber. Thus, by means of the $\hat{\sigma}_{\hat{\boldsymbol{\beta}}}$ and $\hat{\sigma}_{\hat{\boldsymbol{\alpha}}}$ reflections, we have reduced to a minimum the extension needed to locate all distinct LECs. We will take advantage of this in the next section to obtain the ratio of perfect entanglers to all the possible SQGs.

V. ENTANGLING POWER OF SYMMETRIC TWO-QUBIT QUANTUM GATES

A. Expression and properties

The entangling power of a quantum gate acting on a bipartite system is a measure of the ability for these gates to create entangled states from the set of all bipartite separable states.
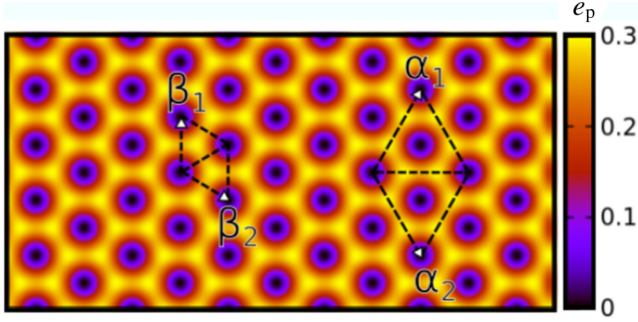
FIG. 3. Entangling power e_p of SQGs on the O plane. The parallelogram spanned by the root vectors $\boldsymbol{\alpha}_1$ and $\boldsymbol{\alpha}_2$ corresponds to the primitive cell. The smaller section defined by $\boldsymbol{\beta}_1$ and $\boldsymbol{\beta}_2$ contains all the possible values of e_p.

In the general two-qubit case [10], the entangling power of a gate $\hat{V}$ [Eq. (4)] is defined as the average of the linear entropy of entanglement $E(|\psi\rangle) = 1 - \mathrm{Tr}(\hat{\rho}_1^2)$ over the set of all separable symmetric two-qubit states with a uniform probability,

$$e_\mathrm{p}(\hat{A}) = \overline{E(\hat{V}\,|\psi_1\rangle \otimes |\psi_2\rangle)}, \qquad (17)$$

with the overbar indicating such an average. Note that we have written e_p as a function of $\hat{A}$, since local transformations do not change the entanglement of a quantum state. The entanglement power is very informative, given that it can be compactly expressed in terms of the two-qubit $|G_1|$ local invariant and can be used as an indicator of whether a quantum gate is a perfect entangler or not [11]. Nevertheless, for SQGs acting on symmetric states only, this expression of the entangling power is not adequate since it takes into account all two-qubit separable states, not necessarily symmetric. Hence, we need to restrict the entangling power definition to symmetric states in order to obtain the correct expression. Accordingly, we define the entangling power of SQGs as

$$e_\mathrm{p}(\hat{U}) = \overline{E(\hat{U}\,|u\rangle \otimes |u\rangle)}, \qquad (18)$$

where $|u\rangle$ is a one-qubit state, as in Sec. II.

We are now going to derive an explicit formula for this expression. First of all, let us consider a uniform distribution of initial $|u, u\rangle$ states, for which the Majorana constellation consists of two stars in the same position. Referring to Appendix B for the details in the derivation, the entangling of SQGs is

$$e_\mathrm{p}(\hat{U}) = \frac{3}{10}(1 - |G|), \qquad (19)$$

with $|G|$ given by the expression (16). It is remarkable that the entangling power obtained can be so compactly expressed in terms of the local invariant $|G|$, which only depends on the trace of matrix $\hat{m}$ [Eq. (12)]. This result resembles that of the entangling power for general two-qubit gates [11], namely, $e_\mathrm{p} = 2(1 - |G_1|)/9$.

The function $e_\mathrm{p}(c_1, c_2, c_3)$ [Eq. (19)] presents minimum and maximum magnitudes at the geometrical points $\boldsymbol{c} = (0, 0, 0)$ and $(-\pi/3, 0, \pi/3)$, which are zero and $\frac{3}{10}$, respectively. As Fig. 3 suggests, these extreme values are also reached at additional points $\boldsymbol{c}$, obtained through symmetry
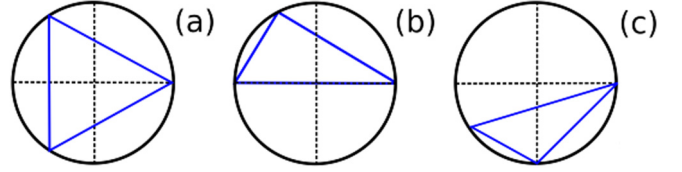

FIG. 4. Convex hull of the matrix $\hat{m}$ associated with SQGs for several entanglement capabilities. The vertices on the unitary circle are defined by the phase of the eigenvalues of $\hat{m}$. (a) Perfect entangler with a maximum value of e_p. (b) Perfect entangler with a minimum value of e_p. (c) Not a perfect entangler. The entangling character of the gate is geometrically determined by the location of the origin, inside (perfect) or outside (nonperfect) the convex hull

operations which are translations along $\boldsymbol{\beta}$ vectors and C_6 rotations about the (1,1,1) axis. Note also that e_p is invariant under translations along this same vector, which means that the same pattern as that shown in Fig. 3 is displayed in planes parallel to the O plane (13).

B. Perfect entanglers

A TQQG $\hat{V}$ is a perfect entangler if it is capable of producing a fully entangled state from a separable one. The condition for this is that the convex hull of eigenvalues of the $\hat{M}$ matrix contains the origin in the $\boldsymbol{c}$ space [13]. For SQGs the same condition holds, applied to the corresponding matrix $\hat{m}$. The proof of this follows along the same lines as in the general case [13]; in order to make the paper more self-contained, we sketch it in Appendix C.

Figure 4 shows the convex hulls of eigenvalues for three distinct cases. The eigenvalues of unitary matrices all have unit length, and thus the circle in the figure is unitary. The vertices of the triangles are defined by the phase of λ_i^2, which are the eigenvalues of $\hat{m}$. In Fig. 4(a) the eigenvalues are separated by $2\pi/3$. This case corresponds to the maximum value $e_\mathrm{p} = \frac{3}{10}$ of the entangling power, since $\lambda_1^2 + \lambda_2^2 + \lambda_3^2 = 0$ and $|G| = 0$. An example of three-level quantum gates, and hence SQGs, with such an entangling power are the SWAP$_{12(23)}$ gates, used in qutrit NMR [5]. In general, the vertices of the triangle for this convex hull are $\phi_1 = \theta + 2\pi/3$, $\phi_2 = \theta - 2\pi/3$, and $\phi_3 = \theta$. In the O plane, the geometrical point is given by $c = \pi(-1, 1, 0)/3$. This corresponds to the white dot in Fig. 5 at the bottom of the blue triangle that, in terms of the root vectors, is written as $(\alpha_1 + \alpha_2)/3$. Thus, all SQGs with $e_\mathrm{p} = \frac{3}{10}$ are locally equivalent to the SWAP$_{12(23)}$ gates.

The case in Fig. 5(b) also represents a convex hull for a perfect entangling SQG, with the requirement that $\lambda_i^2 = -\lambda_j^2$. This makes $|G| = \frac{1}{9}$ and, as a consequence, the entangling power is then $\frac{4}{15}$. In fact, the phase gate $U_{\Lambda_3}(\theta)$ gate [5] has this value of e_p for $\theta = \pi/3$; the U_{Λ_8} [5] phase gate also has this entangling power at $\theta = \pi/\sqrt{3}$. Since any deformation of such a convex hull such that it no longer contains the origin makes e_p less than $\frac{4}{15}$, this value is the minimum such that the corresponding SQGs are perfect entanglers. A SQG with this convex hull can be built with coefficients $\pi(-2, 1, 1)/6$, corresponding to the geometrical point of $\hat{U}_{\Lambda_3}(\pi/3)$ and $\hat{U}_{\Lambda_8}(\pi/\sqrt{3})$. Other coefficients (c_1, c_2, c_3) satisfying this condition can be obtained through symmetry transformations on
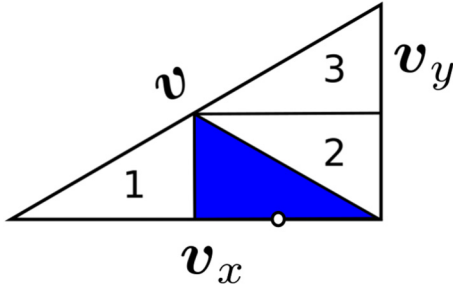
FIG. 5. Weyl chamber of the local-equivalence classes. The blue area contains all the perfect entanglers and it is one-fourth of the triangle. The white dot corresponds to the maximum perfect entangler e_p and is located at $(\frac{2}{3}, 0)$ in the (s_1, s_2) coordinates or, equivalently, on the point $(\boldsymbol{\alpha}_1 + \boldsymbol{\alpha}_2)/3$ (see Fig. 3).

the geometric point just given. The case when the convex hull does not contain the origin is depicted in Fig. 5(c), the SQGs not being perfect entanglers ($e_p < \frac{4}{15}$).

Now that we can classify SQGs as perfect entanglers or not according the geometrical point $\boldsymbol{c}$, we are at a position to calculate the ratio of perfect entanglers to nonperfect entanglers. To do this we will calculate the area of the Weyl chamber whose geometrical points correspond to perfect entangling SQGs. Let us restrict (c_1, c_2, c_3) to the Weyl chamber, as shown in Fig. 5. A comparison with Fig. 3 indicates the following associations: $\boldsymbol{v} = \boldsymbol{\beta}_1 + \boldsymbol{\beta}_2$, $\boldsymbol{v}_x = (\boldsymbol{\alpha}_1 + \boldsymbol{\alpha}_2)/2$, and $\boldsymbol{v}_y = (\boldsymbol{\alpha}_1 - \boldsymbol{\alpha}_2)/6$. As before, the $\boldsymbol{\alpha}_1$ and $\boldsymbol{\alpha}_2$ root vectors are taken as $\pi(-1, 0, 1)$ and $\pi(0, 1, -1)$. Hence, the vectors in Fig. 5 are $\boldsymbol{v} = \frac{\pi}{3}(-2, 1, 1)$, $\boldsymbol{v}_x = \frac{\pi}{2}(-1, 1, 0)$, and $\boldsymbol{v}_y = \frac{\pi}{6}(-1, -1, 2)$. Any geometric point in the Weyl chamber shown in Fig. 5 can be expressed as $\boldsymbol{c} = s_1\boldsymbol{v}_x + s_2\boldsymbol{v}_y$, where $s_1, s_2 \in [0, 1]$ and $s_2 \leqslant s_1$. Upon multiplying the λ^2 eigenvalues by a total phase, its convex hull gets rotated and does not affect whether or not it contains the origin. Thus, regarding $c_1 + c_2 + c_3 = 0$ and setting $\lambda_2^2 = 0$ [see Eqs. (10)], we have

$$\phi_1 = \pi(s_1 + s_2), \tag{20}$$

$$\phi_3 = \pi(s_2 - s_1), \tag{21}$$

where ϕ_1 and ϕ_3 are the phase angles of λ_1^2 and λ_3^2, respectively. With this, a SQG is a perfect entangler if and only if the condition

$$0 \leqslant \phi_1 \leqslant \pi, \quad -\pi \leqslant \phi_3 \leqslant -\pi + \phi_1 \tag{22}$$

holds, where all phases are equivalent modulo 2π. The case $\phi_1 > \pi$ always yields nonperfect entanglers by the imposed conditions on s_1 and s_2 (see the discussion below). Let us analyze all sections of the Weyl chamber to determine whether they are composed of perfect entanglers or not.

Area 1. This area is constrained to the (s_1, s_2) coordinates: $0 \leqslant s_1 < \frac{1}{2}$ and $0 \leqslant s_2 \leqslant s_1$. These inequalities imply that $s_1 + s_2 < 1$, hence $0 \leqslant \phi_1 < \pi$, leaving us in the domain of (22). By substituting ϕ_3 into the right-hand side of (22) we get $s_1 \geqslant \frac{1}{2}$, which is a contradiction given the imposed conditions on s_1 and s_2. Thus, all geometrical points in this section of the Weyl chamber do not correspond to perfect entanglers.

Areas 2 and 3. For these regions we have the following restriction on the (s_1, s_2) coordinates: $\frac{1}{2} < s_1 \leqslant 1$ and $1 - s_1 < s_2 \leqslant s_1$. These imply $\phi_1 > \pi$ and $-\pi < \phi_3 < 0$. Thus, both λ_1^2 and λ_3^2 are on the lower half of the unit circle [see Fig. 4(c)], none of them at π. The convex hull does not contain the origin and the geometrical points do not correspond to perfect entanglers.

Blue area. In this case, the (s_1, s_2) coordinates are constrained by the inequalities: $\frac{1}{2} \leqslant s_1 \leqslant 1$ and $0 \leqslant s_2 \leqslant 1 - s_1$. This implies $\pi \geqslant \phi_1 \geqslant \pi/2$ and consequently we must focus on the expression (22). Inserting Eqs. (20) and (21) into the right inequality of (22), we obtain $-1 \leqslant s_2 - s_1 \leqslant -1 + s_1 + s_2$; $-1 \leqslant s_2 - s_1$ holds trivially, while the right-hand side of the last inequality implies $s_1 \geqslant 1 - s_1$, which holds since we are considering $1 \geqslant s_1 \geqslant \frac{1}{2}$. The expression (22) holds in this case and all the geometrical points contained in the blue area correspond to perfect entanglers.

The blue area occupies one-fourth of the total Weyl chamber. In this sense, the LECs classified as perfect entanglers represent one-fourth of the total SQGs. This contrasts with the general case, in which perfect entanglers are one-half of the total TQQGs. The white dot in Fig. 5 corresponds to perfect entanglers with maximum e_p, while the borders in this area correspond to perfect entanglers with minimum e_p.

It is worth noting at this point that the geometric picture of LECs of SQGs does not trivially arise from that of TQQGs. For example, the Weyl chamber of TQQGs is a tetrahedron that, without loss of generality, has one vertex on the origin O. One of its edges, called the OA_3 edge [13,33], along geometrical points of the form (c, c, c), contains a point P which represents a perfect entangler, the two-qubit SWAP$^{1/2}$ to be specific. Nevertheless, for SQGs, the convex hull on any geometrical point of the form (c, c, c) does not contain the origin, as can be seen from inspection of Eqs. (10) and, as a result, the entangling power is zero along the OA_3 edge. This fundamental difference between the geometry of LECs of SQGs and TQQGs proves that the former is not just a trivial special case of the latter.

We have seen that the SQGs show a simpler geometric description than general two-qubit gates, merely because there is only one local invariant in the former, while the latter has two. This simplification may still hold for a symmetric spaces with a higher number of qubits. For example, one can classify the states of an arbitrary number of symmetric qubit states into distinct entanglement families, while this seems an impossible task for the nonsymmetric case [34]. For this reason it may be worth exploring the geometry of entangling operations in higher dimensional symmetric qubit spaces.

VI. EXAMPLES

In this section we will apply the theory developed so far to three distinct physical models with three-dimensional Hilbert spaces, namely, the anisotropic Heisenberg model, the LMG model, and the two-coupled oscillator model with cross-Kerr interaction. The first one is a two-qubit interaction Hamiltonian acting irreducibly on the symmetric and antisymmetric subspaces, and hence the results developed so far apply and the interpretation of the results is straightforward, in the sense that nonlocal gates produce states of entangled qubit pairs. In

the other two models the formalism also applies; nevertheless, quantum gates classified as nonlocal can produce states with separated Majorana stars that may not be physically entangled. We will further clarify this in the corresponding sections.

We calculate the entangling power as a function of an independent parameter for the three models and find conditions on them to obtain perfect entanglers. By this and inspection of the geometrical points, we find unitary operations locally equivalent to the three-level operations $\hat{U}_{\Lambda_3}(\pi/3)$ and $\hat{U}_{\Lambda_8}(\pi/\sqrt{3})$ and SWAP gates of Ref. [5]. The linear entropy $E(\hat{U}\,|u\rangle \otimes |u\rangle)$ on the Majorana sphere, where each point represents a separable state, is computed and the color will indicate the value of the entanglement measure or the separation between Majorana stars of the final state, depending on the model. We comment on some features of the spatial distribution of entanglement on the Majorana sphere.

A. Anisotropic Heisenberg model with no cross terms

The anisotropic Heisenberg model of two interacting spins is represented by the Hamiltonian [26]

$$\hat{H}_H = \tfrac{1}{2}\big(I_x\hat{\sigma}_x^{(1)}\hat{\sigma}_x^{(2)} + I_y\hat{\sigma}_y^{(1)}\hat{\sigma}_y^{(2)} + I_z\hat{\sigma}_z^{(1)}\hat{\sigma}_z^{(2)}\big), \quad (23)$$

where I_i are the spin coupling constants. This Hamiltonian is composed of the Cartan subalgebra elements of su(4) and hence has a reducible representation into symmetric and antisymmetric subspaces. The symmetric part of the time-evolution operator is, in the Bell basis,

$$\hat{U}_H = \begin{pmatrix} e^{-i(I_x-I_y+I_z)t/2} & 0 & 0 \\ 0 & e^{-i(I_x+I_y-I_z)t/2} & 0 \\ 0 & 0 & e^{-i(-I_x+I_y+I_z)t/2} \end{pmatrix}. \quad (24)$$

From Eq. (23), the $\boldsymbol{c}$ coordinate vector is $(I_x t, I_y t, I_z t)$. The entangling power becomes

$$e_{\mathrm{p}} = \tfrac{2}{15}[\sin^2(I_{xy}t) + \sin^2(I_{yz}t) + \sin^2(I_{xz}t)], \quad (25)$$

where $I_{ij} = I_i - I_j$. Note that for equal spin coupling constants the entangling power is zero, which means that the isotropic Heisenberg model does not have any entangling power on the symmetric two-qubit subspace.

Figure 6(a) shows the entangling power as a function of ωt for the choice of parameters $I_y = 0$ and $I_z = -I_x = \omega$ (left panel), and thus the geometrical points are $\omega t(-1, 0, 1) \parallel \boldsymbol{\alpha}_1$. The maximum values are located at $\omega t = \pi/3, 2\pi/3$, as one would expect, and these are locally equivalent to the SWAP$_{12(23)}$ gates. The minimum e_{p} for which the quantum gate is a perfect entangler is located at $\omega t = \pi/2$.

The sphere on the right shows the linear entropy on the Majorana sphere; we have chosen $\omega t = \pi/3$ in order to obtain maximum entanglement. There are zones on which the quantum gate does not produce entanglement (red spots) and zones where the initial states become symmetric Bell states (blue spots). Even though it is not fully depicted here, there are exactly four low-entanglement zones and four high-entanglement zones, which form a tetrahedron on the sphere. The tetrahedral distribution of the linear entropy on the Majorana is to be expected for any maximum e_{p} perfect entangler, given that they have the same geometrical point and thus
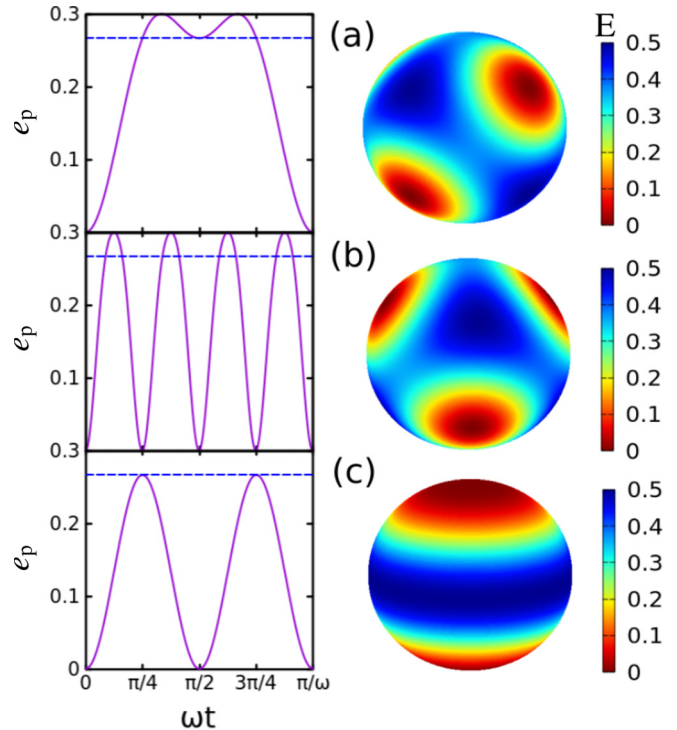

FIG. 6. Shown on the left is the entangling power for (a) the anisotropic Heisenberg model, (b) the Lipkin-Meshkov-Glick model, and (c) the cross-Kerr interaction. The horizontal dashed line indicates the lower bound for perfect entanglers ($e_{\mathrm{p}} = \frac{4}{15}$). Shown on the right is the linear entropy E of the final states obtained by applying $\hat{U}$ to the initial states with degenerate Majorana stars.

the same nonlocal action on the separable set of states. Intriguingly, for the symmetric four-qubit space, whose kets have four stars, there are states that meet different criteria for being the least classical and have also a tetrahedral Majorana constellation [35–37]. The reasons behind the emergence of this pattern of the linear entropy on the Majorana sphere are not evident to us.

B. Lipkin-Meshkov-Glick model

The LMG model was first proposed to study the many-body problem in nuclear physics [27] and has also been useful to model the physics of molecular solids [38,39] and critical phenomena in Bose-Einstein condensates [40]. The Hamiltonian describing the interaction is given by

$$\hat{H}_L = B\hat{J}_z + g_1\hat{J}_z^2 - g_2\hat{J}_x^2. \quad (26)$$

This Hamiltonian commutes with the total angular momentum operator $\boldsymbol{J}^2$, which allows us to fix the j value to unity, for which the model belongs to the su(3) Lie algebra. This model can be written in matrix form as

$$\hat{H}_L = \begin{pmatrix} B + g_1 - \frac{g_2}{2} & 0 & -\frac{g_2}{2} \\ 0 & -g_2 & 0 \\ -\frac{g_2}{2} & 0 & -B + g_1 - \frac{g_2}{2} \end{pmatrix}. \quad (27)$$

The eigenvalues of $\hat{H}_L$ are $\lambda_0 = -g_2$ and $\lambda_\pm = g_1 - g_2/2 \pm \sqrt{B^2 + g_2^2/4}$. The corresponding quantum gates of this system are given by $\exp(-i\hat{H}_L t)$.

This model is a three-level system and as such can be mapped to the symmetric two-qubit space. The isomorphism is given by mapping the angular momentum kets $|1, 1\rangle$, $|1, 0\rangle$, and $|1, -1\rangle$ to the symmetric states $|0, 0\rangle$, $\frac{1}{\sqrt{2}}(|0, 1\rangle + |1, 0\rangle)$, and $|11\rangle$, respectively. With this, the transformation matrix from the spin-1 angular momentum basis to the symmetric Bell basis is given by

$$\hat{T} = \frac{1}{\sqrt{2}} \begin{pmatrix} 1 & 0 & 1 \\ 0 & \sqrt{2}i & 0 \\ i & 0 & -i \end{pmatrix}. \quad (28)$$

The definition of the Bell states should be evident from the matrix above. With this, the absolute square of the local invariant G is given by

$$|G| = \frac{1}{9}\left\{1 + 4G_R \cos\left[2\left(g_1 + \frac{g_2}{2}\right)t\right] + 4G_R^2\right\}, \quad (29)$$

where

$$G_R = 1 - \frac{g_2^2 \sin^2(Rt)}{2R}, \quad R = \sqrt{B^2 + g_2^2/4}.$$

The entangling power is readily obtained through Eq. (19).

As in the anisotropic Heisenberg model, we show the emergence of maximum e_p perfect entanglers. It is not obvious how to achieve this by inspection of Eq. (29), and one has to explore the space of parameters carefully. Figure 6(b) shows the entangling power for the choice of parameters $-2B/7 = g_1/2 = g_2/4 = \omega$, where ω is a fixed frequency. The entangling power displays an oscillating behavior where the maximum e_p is reached at values of ωt closed to $\frac{\pi}{4}(n + \frac{1}{2})$ for some integer $n \geqslant 0$. The geometrical point at the maximum values is $c \approx \pi(-1, 1, 0)/6$, corresponding to a SWAP$_{12(23)}$ gate, as one would expect. For the perfect entanglers with minimum e_p we have checked that these lie on the border of the blue triangle in Fig. 5 but they are not locally equivalent to $\hat{U}_{\Lambda_8}(\pi/3)$.

On the right panel the linear entropy on the Majorana sphere for $\omega t = \pi/8$ is plotted. The colors on the sphere follow the tetrahedronlike patterns, as should be expected for maximum e_p perfect entanglers. The Hilbert space in this model is not bipartite; thus the linear entropy maps should be interpreted as quantifying the separation of Majorana stars.

C. Cross-Kerr interaction

The nonlinear cross-Kerr effect in quantum optics is model by the Hamiltonian [28]

$$\hat{H}_{cK} = \omega_a \hat{a}^\dagger \hat{a} + \omega_b \hat{b}^\dagger \hat{b} + g_{cK} \hat{a}^\dagger \hat{a} \hat{b}^\dagger \hat{b}. \quad (30)$$

This Hamiltonian is an interacting two-boson model that conserves the total number of excitations $\hat{N} = (\hat{a}^\dagger \hat{a} + \hat{b}^\dagger \hat{b})$. An arbitrary state in this Hilbert space is given by

$$|\psi\rangle = \sum_{m=-n/2}^{n/2} c_m \frac{\hat{a}^{\dagger(n/2+m)} \hat{b}^{\dagger(n/2-m)}}{\sqrt{(n/2+m)!(n/2-m)!}} |0, 0\rangle$$

$$= \sum_m c_m |n/2 + m, n/2 - m\rangle.$$

In this expression $|n_a, n_b\rangle$ denotes a tensor product of Fock states with n_a and n_b number of excitations, respectively. By transforming the Hamiltonian via the Schwinger operators

of the angular momentum [41], it is easily seen that $\hat{N}/2$ equals the total angular momentum j of the resulting Hamiltonian. Let us work in the $j = 1$ representation. The cross-Kerr Hamiltonian becomes

$$\hat{H}_{cK} = (\omega_a - \omega_b)\hat{J}_z - g_{cK}\hat{J}_z^2,$$

The cross-Kerr interaction can be modeled as a LMG model after the identification $B = \omega_a - \omega_b$, $g_1 = -g_{cK}$, and $g_2 = 0$. Also, the mapping from the two-boson Hilbert space to the angular momentum basis in the spin-1 representation is given by $|2, 0\rangle, |1, 1\rangle, |0, 2\rangle \to |1\rangle, |0\rangle, |-1\rangle$. The entangling power is then easily obtained from Eqs. (29) and (19) and the transformation matrix (28),

$$e_p = \frac{4}{15} \sin^2(g_{cK}t).$$

Figure 6(c) shows the entangling power for a choice of parameters $B = g_1/2 = \omega$. The entangling power has an oscillating behavior that never reaches the maximum possible value. The eigenvalues of the $\hat{m}$ matrix are $e^{-ig_{cK}t}$, $e^{-ig_{cK}t}$, and 1. There is a pair of degenerate eigenvalues, and thus the convex hull contains the origin only when the vertices are on antipodal positions on the unit circle, which gives the minimum e_p for which $\hat{U}$ is a perfect entangler. It can be checked that the geometrical points of the perfect entanglers are located at $\pi(-2, 1, 1)/6$; hence they are locally equivalent to the $\hat{U}_{\Lambda_8}(\pi/3)$ and $\hat{U}_{\Lambda_8}(\pi/\sqrt{3})$ qutrit gates.

The linear entropy on the Majorana sphere is depicted on the right, which is very different from the spheres in Figs. 6(a) and 6(b). The antipodal low entangling spots on the sphere with a high entangling zone between them is a general feature of quantum gates with $e_p = \frac{4}{15}$, as we have seen from distinct numerical calculations, without regard to the details of the Hamiltonian. As in the LMG model, the linear entropy quantifies the separation between Majorana stars. The model (30) admits genuine entanglement, since its Hilbert space is bipartite. The linear entropy in Fig. 6(c) represents the separation between the Majorana stars, but not the entanglement of the states in the two-boson space. Take $|1, 1\rangle$, for example. This state corresponds to $|0\rangle$ in the Schwinger representation of the model. By the isomorphism between angular momentum spin-1 kets and symmetric states, we have that $|1, 1\rangle$ corresponds to $(|01\rangle + |10\rangle)/\sqrt{2}$ in the symmetric two-qubit basis. For this reason we must be cautious when applying this formalism to three-level systems coming from a two-boson interacting model, in that states with separate Majorana stars may still be separable in the original Hilbert space.

VII. CONCLUSION

We have given a geometric classification of the LECs of SQGs, which turns out to be a plane with hexagonal symmetry. There we have identified the Weyl chamber, which is the minimum area that contains all distinct LECs. This geometric description contrasts with the general two-qubit case, for which the geometry is three dimensional. The entangling power for SQGs is obtained in terms of the local invariant. As was done in the general two-qubit case in Ref. [13], we gave conditions for which a SQG is a perfect entangler and have found that the perfect entanglers are one-fourth of all possible SQGs. Along this line, we also found that perfect entanglers

must have $e_{\mathrm{p}} \geqslant \frac{4}{15}$. It was stressed that LECs of SQGs do not arise trivially from those of TQQGs, since there exist geometrical points corresponding to perfect entanglers in the latter case (TQQGs) that yield gates with zero e_{p} in the former (SQGs). The theoretic framework developed herein can be applied to any three-level system, whether it is bipartite or not. The entangling power then refers to the capability of quantum gates to perform transformations that do not act as SO(3) rotations on the Majorana constellation such as some phase gates, e.g., SWAP$_{12}$ and SWAP$_{23}$ gates [5]. Finally, the formalism we developed was applied to three physical models, namely, the anisotropic Heisenberg model [26], the Lipkin-Meshkov-Glick model [27], and two coupled quantized oscillators with cross-Kerr interaction [28], and we found some conditions on the Hamiltonian parameters to generate perfect entangling three-level quantum gates. The last two models are not physically symmetric two-qubit systems, but only three-level systems that can be mapped onto such systems. On the LMG model it was possible to obtain maximum e_{p} perfect entanglers, which are locally equivalent to the SWAP$_{12(23)}$ operations. In the coupled-quantized-oscillator model, we obtained minimum e_{p} perfect entanglers locally equivalent to the $\hat{U}_{\Lambda_3}(\pi/3)$ and $\hat{U}_{\Lambda_8}(\pi/\sqrt{3})$ qutrit gates. Additional examples might include solid-state systems or optical analogs, such as assemblies of three quantum dots with few electrons used to study coherent control of quantum states [42], Landau-Zener-Stückelberg interferometry [43], or quantum transport [44], among other properties.

APPENDIX A: CARTAN DECOMPOSITION OF THE su(3) LIE ALGEBRA

In this Appendix we show that the su(3) Lie algebra has a Cartan decomposition, which allows us to write the appropriate *KAK* decomposition of the group (as we mentioned in Sec. III). For this decomposition to hold the Lie algebra must be written as a direct sum (in the sense of vector spaces) of two sets, namely, $\mathfrak{k}$ and $\mathfrak{p}$, whose elements are orthogonal with respect to the Killing form [13]. The Killing form is defined by $B(\hat{X}, \hat{Y}) = \mathrm{Tr}(\mathrm{ad}_{\hat{X}} \mathrm{ad}_{\hat{Y}})$, where $\mathrm{ad}_{\hat{X}}$ is the adjoint representation of $\hat{X} \in \mathfrak{g}$ [45]. Then, if it is always true that $B(\hat{X}, \hat{Y}) = 0$ for any two elements $\hat{X} \in \mathfrak{k}$ and $\hat{Y} \in \mathfrak{p}$, then $\mathfrak{k} = \mathfrak{p}^{\perp}$ and the two spaces are said to be orthogonal. We now give the following definition [13].

Definition 1 (Cartan decomposition of a Lie algebra). Let $\mathfrak{g}$ be a semisimple Lie algebra and let the decomposition $\mathfrak{g} = \mathfrak{k} \oplus \mathfrak{p}$, with $\mathfrak{k} = \mathfrak{p}^{\perp}$ and the commutation relations

$$[\mathfrak{k}, \mathfrak{k}] \in \mathfrak{k}, \quad [\mathfrak{k}, \mathfrak{p}] \in \mathfrak{p}, \quad [\mathfrak{p}, \mathfrak{p}] \in \mathfrak{k}. \tag{A1}$$

The Lie algebra $\mathfrak{g}$ is said to have a Cartan decomposition.

TABLE I. Commutation relations of the su(3) algebra elements.

$i[\hat{X}_i, \hat{X}_j]$	$\hat{J}_x$	$\hat{J}_y$	$\hat{J}_z$	$\hat{h}_1$	$\hat{h}_2$	$\hat{L}_1$	$\hat{L}_2$	$\hat{L}_3$
$\hat{J}_x$	0	$-\hat{J}_z$	$\hat{J}_y$	$\hat{L}_3$	$-2\hat{L}_3$	$\hat{L}_2$	$-\hat{L}_1$	$\hat{h}_2$
$\hat{J}_y$	$\hat{J}_z$	0	$-\hat{J}_x$	$-2\hat{L}_2$	$\hat{L}_2$	$\hat{L}_3$	$\hat{h}_1$	$\hat{L}_1$
$\hat{J}_z$	$-\hat{J}_y$	$\hat{J}_x$	0	$\hat{L}_1$	$\hat{L}_1$	$-\hat{h}_3$	$-\hat{L}_3$	$\hat{L}_2$
$\hat{h}_1$	$-\hat{L}_3$	$2\hat{L}_2$	$-\hat{L}_1$	0	0	$\hat{J}_z$	$-2\hat{J}_y$	$\hat{J}_x$
$\hat{h}_2$	$2\hat{L}_3$	$-\hat{L}_2$	$-\hat{L}_1$	0	0	$\hat{J}_z$	$\hat{J}_y$	$-2\hat{J}_x$
$\hat{L}_1$	$-\hat{L}_2$	$-\hat{L}_3$	$\hat{h}_3$	$-\hat{J}_z$	$-\hat{J}_z$	0	$-\hat{J}_x$	$\hat{J}_y$
$\hat{L}_2$	$\hat{L}_1$	$-\hat{h}_1$	$\hat{L}_3$	$2\hat{J}_y$	$-\hat{J}_y$	$\hat{J}_x$	0	$-\hat{J}_z$
$\hat{L}_3$	$-\hat{h}_2$	$-\hat{L}_1$	$-\hat{L}_2$	$-\hat{J}_x$	$2\hat{J}_x$	$-\hat{J}_y$	$\hat{J}_z$	0

The su(3) Lie algebra is semisimple [32]. Now let us write the following linearly independent matrices that span the su(3) Lie algebra:

$$\hat{J}_x = \frac{1}{\sqrt{2}} \begin{pmatrix} 0 & 1 & 0 \\ 1 & 0 & 1 \\ 0 & 1 & 0 \end{pmatrix}, \quad \hat{L}_1 = i \begin{pmatrix} 0 & 0 & -1 \\ 0 & 0 & 0 \\ 1 & 0 & 0 \end{pmatrix},$$

$$\hat{J}_y = \frac{i}{\sqrt{2}} \begin{pmatrix} 0 & -1 & 0 \\ 1 & 0 & -1 \\ 0 & 1 & 0 \end{pmatrix}, \quad \hat{L}_2 = \frac{1}{\sqrt{2}} \begin{pmatrix} 0 & 1 & 0 \\ 1 & 0 & -1 \\ 0 & -1 & 0 \end{pmatrix},$$

$$\tag{A2a}$$

$$\hat{J}_z = \begin{pmatrix} 1 & 0 & 0 \\ 0 & 0 & 0 \\ 0 & 0 & -1 \end{pmatrix}, \quad \hat{L}_3 = \frac{i}{\sqrt{2}} \begin{pmatrix} 0 & -1 & 0 \\ 1 & 0 & 1 \\ 0 & -1 & 0 \end{pmatrix},$$

$$\hat{h}_1 = \frac{1}{2} \begin{pmatrix} 1 & 0 & -1 \\ 0 & -2 & 0 \\ -1 & 0 & 1 \end{pmatrix}, \quad \hat{h}_2 = \frac{1}{2} \begin{pmatrix} -1 & 0 & -1 \\ 0 & 2 & 0 \\ -1 & 0 & -1 \end{pmatrix}.$$

$$\tag{A2b}$$

In these equations the $\hat{h}_1$ and $\hat{h}_2$ commute and form the Cartan subalgebra. The basis for these matrices is labeled as $|1\rangle, |0\rangle, |-1\rangle$, which corresponds to the $|00\rangle, (|01\rangle + |10\rangle)/\sqrt{2}, |11\rangle$ symmetric basis.

Lumping together the matrices above into the sets $\mathfrak{k} = \{\hat{J}_i\}$ and $\mathfrak{p} = \{\hat{L}_j, \hat{h}_k\}$, we obtain the commutation relations in Table I. There we define $\hat{h}_3 = \hat{h}_1 + \hat{h}_2$. Hence, it is easily checked that $[\mathfrak{k}, \mathfrak{k}] \in \mathfrak{k}$, $[\mathfrak{k}, \mathfrak{p}] \in \mathfrak{p}$, and $[\mathfrak{p}, \mathfrak{p}] \in \mathfrak{k}$.

The second important property is that the elements of $\mathfrak{k}$ are orthogonal to the elements of $\mathfrak{p}$ with respect to the Killing form $B(\hat{X}, \hat{Y})$. This can be directly checked with the $\mathfrak{k}$ and $\mathfrak{p}$ sets chosen here. We have then given a Cartan decomposition of the su(3) Lie algebra, and hence any three-level quantum gate $\hat{U} \in \mathrm{SU}(3)$ can be written as $\hat{k}_1 \hat{B} \hat{k}_2$ [30], with

$$\hat{k} = e^{-i\theta \hat{\mathbf{n}} \cdot \hat{\mathbf{J}}}, \quad \hat{B} = e^{-i(x_1 \hat{h}_1 + x_2 \hat{h}_2)},$$

where x_1 and x_2 are real coefficients.

Before finishing this Appendix, let us note that the su(3) Lie algebra elements in (A2) can be obtained by symmetric linear combinations of the SU(4) generators, given by all the tensor products of the Pauli matrices [13]. For this let us

introduce the transformation matrix

$$
\hat{T}^\dagger = \begin{pmatrix} 1 & 0 & 0 & 0 \\ 0 & \frac{1}{\sqrt{2}} & \frac{1}{\sqrt{2}} & 0 \\ 0 & 0 & 0 & 1 \\ 0 & \frac{1}{\sqrt{2}} & -\frac{1}{\sqrt{2}} & 0 \end{pmatrix}, \tag{A3}
$$

transforming the computational basis into a symmetric part (first three rows) and an antisymmetric part (last row). Thus, an element of $\hat{X} \in su(4)$ transforms to $\hat{T}^\dagger \hat{X} \hat{T}$ in that basis. We have the associations

$$
\frac{1}{2}\hat{T}^\dagger(\hat{\sigma}_x^{(1)}\mathbb{1}^{(2)} + \mathbb{1}^{(1)}\hat{\sigma}_x^{(2)})\hat{T} = \begin{pmatrix} \hat{J}_x & 0 \\ 0 & 0 \end{pmatrix}, \tag{A4a}
$$

$$
\frac{1}{2}\hat{T}^\dagger(\hat{\sigma}_y^{(1)}\mathbb{1}^{(2)} + \mathbb{1}^{(1)}\hat{\sigma}_y^{(2)})\hat{T} = \begin{pmatrix} \hat{J}_y & 0 \\ 0 & 0 \end{pmatrix}, \tag{A4b}
$$

$$
\frac{1}{2}\hat{T}^\dagger(\hat{\sigma}_z^{(1)}\mathbb{1}^{(2)} + \mathbb{1}^{(1)}\hat{\sigma}_z^{(2)})\hat{T} = \begin{pmatrix} \hat{J}_z & 0 \\ 0 & 0 \end{pmatrix}, \tag{A4c}
$$

$$
\frac{1}{2}\hat{T}^\dagger(\hat{\sigma}_x^{(1)}\hat{\sigma}_y^{(2)} + \hat{\sigma}_y^{(1)}\hat{\sigma}_x^{(2)})\hat{T} = \begin{pmatrix} \hat{L}_1 & 0 \\ 0 & 0 \end{pmatrix}, \tag{A4d}
$$

$$
\frac{1}{2}\hat{T}^\dagger(\hat{\sigma}_y^{(1)}\hat{\sigma}_z^{(2)} + \hat{\sigma}_z^{(1)}\hat{\sigma}_y^{(2)})\hat{T} = \begin{pmatrix} \hat{L}_2 & 0 \\ 0 & 0 \end{pmatrix}, \tag{A4e}
$$

$$
\frac{1}{2}\hat{T}^\dagger(\hat{\sigma}_x^{(1)}\hat{\sigma}_z^{(2)} + \hat{\sigma}_z^{(1)}\hat{\sigma}_x^{(2)})\hat{T} = \begin{pmatrix} \hat{L}_3 & 0 \\ 0 & 0 \end{pmatrix}, \tag{A4f}
$$

$$
\frac{1}{2}\hat{T}^\dagger(-\hat{\sigma}_x^{(1)}\hat{\sigma}_x^{(2)} + \hat{\sigma}_z^{(1)}\hat{\sigma}_z^{(2)})\hat{T} = \begin{pmatrix} \hat{h}_1 & 0 \\ 0 & 0 \end{pmatrix}, \tag{A4g}
$$

$$
\frac{1}{2}\hat{T}^\dagger(\hat{\sigma}_y^{(1)}\hat{\sigma}_y^{(2)} - \hat{\sigma}_z^{(1)}\hat{\sigma}_z^{(2)})\hat{T} = \begin{pmatrix} \hat{h}_2 & 0 \\ 0 & 0 \end{pmatrix}. \tag{A4h}
$$

The generators of reducible two-qubit operations can be mapped into the su(3) generators by a unitary transformation. As seen from the expressions above, these are comprised of symmetric linear combinations of the Pauli matrices, which ensures maintenance of the particle exchange symmetry during the dynamics.

APPENDIX B: DERIVATION OF THE ENTANGLING POWER FOR SQGs

To derive an explicit expression for the entangling power of SQGs, we first compute $\mathrm{Tr}[\hat{\rho}_1^2]$ and then integrate it over the unit sphere. The pure state density matrix obtained after applying a SQG $\hat{U}$ to a symmetric two-qubit separable state $|u, u\rangle$ is given by $\hat{U}|u, u\rangle\langle u, u|\hat{U}^\dagger$. Since we are interested in this quantity in order to calculate the entropy of entanglement, the local contributions to the quantum gate $\hat{U}$ can be omitted and hence

$$
\hat{\rho} = \hat{A}|u, u\rangle\langle u, u|\hat{A}^\dagger.
$$

Now, by expressing $|u, u\rangle$ in the Bell basis through the matrix $\hat{Q}^\dagger$ [Eq. (8)], we find

$$
\hat{Q}^\dagger|u, u\rangle = \frac{1}{\sqrt{2}}(a \quad ib \quad -ic \quad 0)^T,
$$

where $a = \cos\phi - i\sin\phi\cos\theta$, $b = i\sin\theta$, and $c = -i\sin\phi + \cos\phi\cos\theta$. By transforming the $\hat{A}$ matrix to the Bell basis too, after some manipulations we get the

density matrix

$$
\hat{\rho} = \frac{1}{4}\begin{pmatrix} |A|^2 & AB^* & AB^* & AC^* \\ A^*B & |B|^2 & |B|^2 & BC^* \\ A^*B & |B|^2 & |B|^2 & BC^* \\ A^*C & BC^* & BC^* & |C|^2 \end{pmatrix},
$$

where the complex coefficients in the matrix elements are $A = \lambda_1 a - i\lambda_3 c$, $B = \lambda_2 b$, and $C = \lambda_1 a + i\lambda_3 c$, with the λ_i factors given in Eqs. (10). After reducing this matrix on one of the subsystems, we obtain

$$
\mathrm{Tr}\hat{\rho}_1^2 = \frac{1}{16}[(|A|^2 + |B|^2)^2 + (|B|^2 + |C|^2)^2 + 2|AB^* + BC^*|^2].
$$

What remains is to average this expression over all the possible symmetric separate states (degenerate Majorana constellations), where each state is equally likely to be obtained,

$$
\overline{\mathrm{Tr}\hat{\rho}_1^2} = \frac{1}{4\pi}\int_{\mathcal{A}}\left[\mathrm{Tr}\hat{\rho}_1^2\right]\sin\theta\, d\theta\, d\phi,
$$

with integration performed over the surface $\mathcal{A}$ of the unit sphere. After a long but straightforward algebra, we obtain, from (18),

$$
e_p = \tfrac{2}{15}[\sin^2(c_{12}) + \sin^2(c_{23}) + \sin^2(c_{31})],
$$

which can be recast in the form (19) by using the local invariant expression (16).

APPENDIX C: CONDITION FOR A PERFECT ENTANGLER

In order to determine the values of e_p for which a SQG is a perfect entangler, we need first a theorem based on the eigenvalues of the matrix $\hat{m}$. The proof is very similar to that given in Ref. [13] for the general two-qubit case, with the appropriate changes to focus on the symmetric case. First, we recall the definition of a convex hull.

Definition 2 (convex hull). The convex hull of $n + 1$ points $\boldsymbol{p}_0, \boldsymbol{p}_1, \ldots, \boldsymbol{p}_n \in \mathbb{R}^n$ is given by the set of all vectors of the form $\sum_{i=0}^n \theta_i \boldsymbol{p}_i$, where θ_i are non-negative real numbers satisfying $\sum_{i=0}^n \theta_i = 1$.

Now we state and prove the following theorem.

Theorem 1 (perfect entanglers). A symmetric two-qubit gate $\hat{U}$ is a perfect entangler if and only if the convex hull of eigenvalues of $\hat{m}$ contains zero.

Proof. As explained in Sec. III, a general symmetric two-qubit gate can be decomposed as $\hat{U} = \hat{K}_1^{(s)}\hat{A}^{(s)}\hat{K}_2^{(s)}$, where $\hat{K}^{(s)} \in SU(2)$ in the spin-1 representation. Given a symmetric separable two-qubit state $|\psi_o\rangle = (a\ b\ b\ c)^T$, it is obtained for the concurrence [1] of the state $\hat{U}|\psi_o\rangle$ that $C(\hat{U}|\psi_o\rangle) = C(\hat{A}|\psi_o\rangle)$, and thus for $\hat{U}$ to be a perfect entangler $\hat{A}$ has to be a perfect entangler; we have also used $\hat{A}|\psi_o\rangle = \hat{A}^{(s)}|\psi_o\rangle$, since $|\psi_o\rangle$ is symmetric. Explicitly, $C(\hat{A}|\psi_o\rangle) = \overline{\langle\psi_o|}\hat{A}^T\hat{P}\hat{A}|\psi_o\rangle$, where $\hat{P} = -\hat{\sigma}_y \otimes \hat{\sigma}_y$. This expression can be rewritten in terms of Bell states as $C(\hat{A}|\psi_o\rangle) = \overline{\langle\psi_o|\hat{Q}}\hat{F}^2(\hat{Q}^\dagger|\psi_o\rangle)$, where we have used the matrix $\hat{Q}$ (8) and the result $\hat{Q}^T\hat{P}\hat{Q} = \mathbb{1}$; the operator $\hat{F}$ is $\hat{Q}^\dagger\hat{A}\hat{Q}$. Let $\hat{Q}^\dagger|\psi_o\rangle = |\phi\rangle$. Since $|\psi_o\rangle$ is a nonentangled state, we have $C(|\psi_o\rangle) = \overline{\langle\psi_o|}\hat{P}|\psi_o\rangle = \overline{\langle\phi|}\hat{Q}^T\hat{P}\hat{Q}|\phi\rangle = \overline{\langle\phi|}\mathbb{1}|\phi\rangle =$

0, which implies

$$\phi_1^2 + \phi_2^2 + \phi_3^2 = 0, \tag{C1}$$

where only three expansion coefficients appear, since $|\psi_o\rangle$ is a symmetric state and thus has no projection on the antisymmetric axis. For $\hat{A}$ to be a perfect entangler, the concurrence of $\hat{A}|\psi_o\rangle$ must equal unity, which along with the normalization condition yields $|\phi_1^2\lambda_1^2 + \phi_2^2\lambda_2^2 + \phi_3^2\lambda_3^2| = |\phi_1^2\lambda_1^2| + |\phi_2^2\lambda_2^2| + |\phi_3^2\lambda_3^2|$, where the eigenvalues λ_i are given in Eqs. (10). This equation holds if and only if there exists a number $\theta \in [0, 2\pi)$

such that $\phi_j^2\lambda_j^2 = |\phi_j|^2 e^{i2\theta}$, $j = 1, 2, 3, 4$. From the above discussion and Eq. (C1) we get

$$\begin{aligned}
\phi_1^2 + \phi_2^2 + \phi_3^2 &= e^{i2\theta}\left(\frac{|\phi_1|^2}{\lambda_1^2} + \frac{|\phi_2|^2}{\lambda_2^2} + \frac{|\phi_3|^2}{\lambda_3^2} \right) \\
&= e^{i2\theta}\left(|\phi_1|^2\overline{\lambda_1^2} + |\phi_2|^2\overline{\lambda_2^2} + |\phi_3|^2\overline{\lambda_3^2} \right) \\
&= 0.
\end{aligned}$$

By complex conjugation of the last equality, it follows that the convex hull of the eigenvalues of $m(\hat{U})$ contains the origin. The converse statement can be done following Ref. [13].

---

[1] J. Audrescht, *Entangled Systems* (Wiley, New York, 2007).

[2] R. Horodecki, P. Horodecki, M. Horodecki, and K. Horodecki, Rev. Mod. Phys. **81**, 865 (2009).

[3] A. Muthukrishnan and C. R. Stroud, Phys. Rev. A **62**, 052309 (2000).

[4] M. Jerger, Y. Reshitnyk, M. Oppliger, A. Potočnik, M. Mondal, A. Wallraff, K. Goodenough, S. Wehner, K. Juliusson, N. K. Langford, and A. Fedorov, Nat. Commun. **7**, 12930 (2016).

[5] S. Dogra, K. Dorai, and Arvind, J. Phys. B **51**, 045505 (2018).

[6] J. Randall, A. M. Lawrence, S. C. Webster, S. Weidt, N. V. Vitanov, and W. K. Hensinger, Phys. Rev. A **98**, 043414 (2018).

[7] E. Majorana, Nuovo Cimento **9**, 43 (1932).

[8] A. R. U. Devi, Sudha, and A. K. Rajagopal, Quantum Inf. Process. **11**, 685 (2012).

[9] H. D. Liu and L. B. Fu, Phys. Rev. A **94**, 022123 (2016).

[10] P. Zanardi, C. Zalka, and L. Faoro, Phys. Rev. A **62**, 030301(R) (2000).

[11] S. Balakrishnan and R. Sankaranarayanan, Phys. Rev. A **82**, 034301 (2010).

[12] A. T. Rezakhani, Phys. Rev. A **70**, 052313 (2004).

[13] J. Zhang, J. Vala, S. Sastry, and K. B. Whaley, Phys. Rev. A **67**, 042313 (2003).

[14] K. Bergmann, H. Theuer, and B. W. Shore, Rev. Mod. Phys. **70**, 1003 (1998).

[15] K. S. Kumar, A. Vepsäläinen, S. Danilin, and G. S. Paraoanu, Nat. Commun. **7**, 10628 (2016).

[16] S. Dogra, A. Vepsäläinen, and G. S. Paraoanu, Phys. Rev. Research **2**, 043079 (2020).

[17] T. Ohmi and K. Machida, J. Phys. Soc. Jpn. **67**, 1822 (1998).

[18] Q. Chang, Q. Qin, W. Zhang, L. You, and M. S. Chapman, Nat. Phys. **1**, 111 (2005).

[19] T.-L. Ho, Phys. Rev. Lett. **81**, 742 (1998).

[20] B. P. Lanyon, T. J. Weinhold, N. K. Langford, J. L. O'Brien, K. J. Resch, A. Gilchrist, and A. G. White, Phys. Rev. Lett. **100**, 060504 (2008).

[21] S. Dogra, Arvind, and K. Dorai, Phys. Lett. A **378**, 3452 (2014).

[22] E. T. Campbell, H. Anwar, and D. E. Browne, Phys. Rev. X **2**, 041021 (2012).

[23] S. Muralidharan, C.-L. Zou, L. Li, J. Wen, and L. Jiang, New J. Phys. **19**, 013026 (2017).

[24] Y.-H. Luo, H.-S. Zhong, M. Erhard, X.-L. Wang, L.-C. Peng, M. Krenn, X. Jiang, L. Li, N.-L. Liu, C.-Y. Lu, A. Zeilinger, and J.-W. Pan, Phys. Rev. Lett. **123**, 070505 (2019).

[25] M. S. Blok, V. V. Ramasesh, T. Schuster, K. O'Brien, J. M. Kreikebaum, D. Dahlen, A. Morvan, B. Yoshida, N. Y. Yao, and I. Siddiqi, Phys. Rev. X **11**, 021010 (2021).

[26] A. Abliz, H. J. Gao, X. C. Xie, Y. S. Wu, and W. M. Liu, Phys. Rev. A **74**, 052105 (2006).

[27] H. Lipkin, N. Meshkov, and A. Glick, Nucl. Phys. **62**, 188 (1965).

[28] M. Bhattacharya and H. Shi, Am. J. Phys. **81**, 267 (2013).

[29] H. D. Liu and L. B. Fu, Phys. Rev. Lett. **113**, 240403 (2014).

[30] A. W. Knapp, *Lie Groups Beyond an Introduction* (Birkhäuser, Boston, 1996).

[31] Y. Makhlin, Quantum Inf. Process. **1**, 243 (2002).

[32] B. Hall, *Lie Groups, Lie Algebras and Representations: An Elementary Introduction* (Springer International, Cham, 2015).

[33] S. Balakrishnan and R. Sankaranarayanan, Phys. Rev. A **79**, 052339 (2009).

[34] T. Bastin, S. Krins, P. Mathonet, M. Godefroid, L. Lamata, and E. Solano, Phys. Rev. Lett. **103**, 070503 (2009).

[35] J. Zimba, Electron. J. Theor. Phys. **3**, 143 (2006).

[36] O. Giraud, P. Braun, and D. Braun, New J. Phys. **12**, 063005 (2010).

[37] G. Björk, A. B. Klimov, P. de la Hoz, M. Grassl, G. Leuchs, and L. L. Sánchez-Soto, Phys. Rev. A **92**, 031801(R) (2015).

[38] A. Garg, Europhys. Lett. **22**, 205 (1993).

[39] J. Campos and J. Hirsch, Rev. Mex. Fis. S **57**, 56 (2011).

[40] P. Ribeiro, J. Vidal, and R. Mosseri, Phys. Rev. Lett. **99**, 050402 (2007).

[41] J. Sakurai and J. Napolitano, *Modern Quantum Mechanics* (Addison-Wesley, Reading, 1994).

[42] T. Brandes, Phys. Rep. **408**, 315 (2005).

[43] F. Gallego-Marcos, R. Sánchez, and G. Platero, Phys. Rev. B **93**, 075424 (2016).

[44] I. Maldonado, J. Villavicencio, L. D. Contreras-Pulido, E. Cota, and J. A. Maytorena, Phys. Rev. B **97**, 195310 (2018).

[45] N. Jeevanjee, *An Introduction to Tensors and Group Theory for Physicists.*, 2nd ed. (Birkhäuser, Boston, 2015).